Journal of
Nanophotonics

SPIEDigitalLibrary.org/jnp

Thin-film growth dynamics with shadowing and re-emission effects

Tansel Karabacak

SPIE

Thin-film growth dynamics with shadowing and re-emission effects

Tansel Karabacak
University of Arkansas at Little Rock, Department of Applied Science, Little Rock, Arkansas 72204, USA
txkarabacak@ualr.edu

Abstract. Growth dynamics of thin-films involves both shadowing and re-emission effects. Shadowing can originate from obliquely incident atoms being preferentially deposited on hills of the surface, which leads to a long range geometrical effect, as well as from an atomic shadowing process that can occur even during normal angle deposition. Re-emission effect is a result of nonsticking atoms, which can bounce off from hills and deposit on valleys of the surface. In the case of an energetic incident flux, re-emission can also originate from a resputtering process that includes a surface atom being knocked off by an incident ion/atom followed by redeposition to another surface point. Due to their long-range nonlocal nature, both the shadowing effect (which tries to roughen the surface) and re-emission effect (which has a smoothening effect) have been shown to be more dominant over local effects such as surface diffusion, and have been proven to be critical processes in accurately determining the dynamic evolution of surface roughness. Recent Monte Carlo simulation methods that involve shadowing, re-emission, surface diffusion, and noise effects successfully predicted many experimentally relevant surface roughness evolution results reported in the literature. For example, root-mean-square surface roughness (ω) of Monte Carlo simulated thin-films have evolved with time t according to a power law behavior $\omega \sim t^{\beta}$, with β values ranging from about 0 to 1 for a growth with strong re-emission effects (i.e., low sticking coefficients) and a growth with dominant shadowing effects (i.e., with high sticking coefficients), respectively. Potential future thin-film growth modeling studies are also discussed. These include advanced simulation approaches that can incorporate atomistic details of physical and chemical processes and a recently developed network growth model that can potentially capture some universal aspects of thin-film growth dynamics independent of the details of growth process. *© 2011 Society of Photo-Optical Instrumentation Engineers (SPIE)*. [DOI: 10.1117/1.3543822]

Keywords: thin-film growth modeling; surface roughness; growth dynamics; shadowing effect; re-emission effect; resputtering; scaling exponents; growth exponent; simulations.

Paper 10023VRR received Apr. 5, 2010; revised manuscript received Dec. 13, 2010; accepted for publication Dec. 15, 2010; published online Mar. 4, 2011.

1 Introduction

Thin-film coatings have been the focus of many researchers due to their wide spread applications in industries including optoelectronics, microelectronics, MEMS, and nanoelectromechanical systems (NEMS). Thin-films have thickness typically in the nano- to micro-scales and are mostly grown using vacuum deposition techniques.[1–3] Surface morphology of thin-film controls many important physical and chemical properties of the coating. It is therefore of great interest to understand and control the evolution of the surface morphology during thin-film growth.

Figure 1 shows some of the most commonly employed deposition techniques[4] thermal evaporation, sputter deposition, CVD, and more recently oblique angle deposition (also named glancing angle deposition or GLAD). Different than others, the oblique angle deposition technique[5–12]

1934-2608/2011/$25.00 © 2011 SPIE

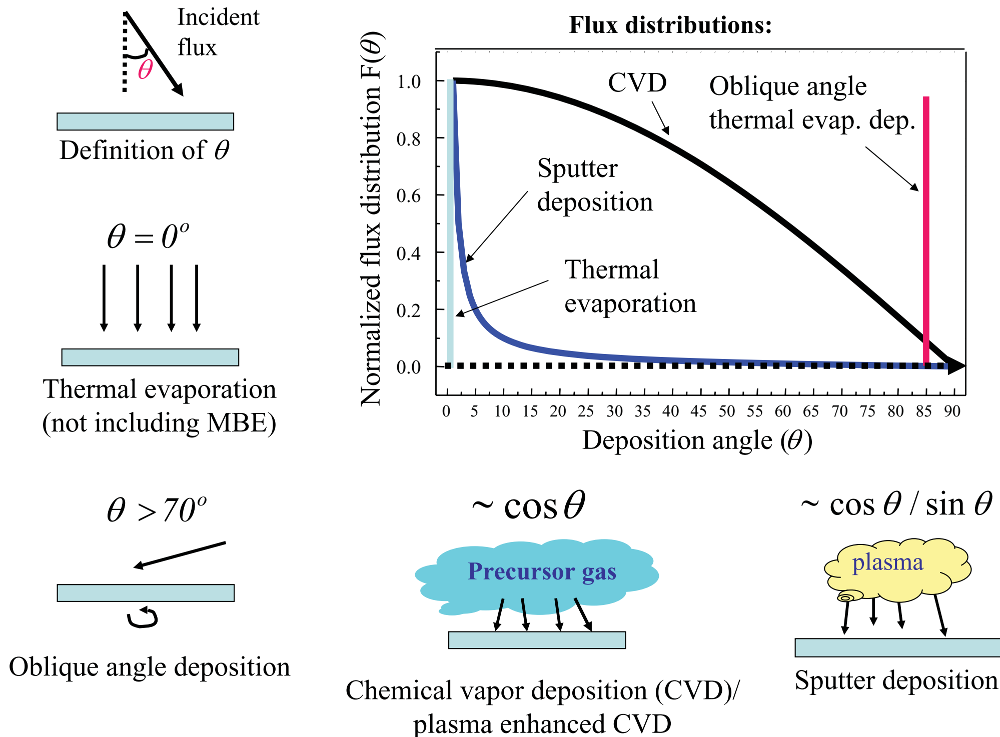

Fig. 1 Schematic diagrams showing the geometries of several commonly employed thin-film deposition techniques. The inset is a plot of the incident flux distribution of the atoms arriving at the substrate in different deposition techniques. Reprinted with permission from Ref. 4. Copyright 2003, Materials Research Society.

is typicallyused for the growth of nanostructured arrays of rods and springs through a physical self-assembly process. Here in this paper, we do not include the MBE technique that involves detailed interactions between the newly deposited adatoms and the surface steps.[13] (These detailed interactions can generate a separate class of morphologies.) Included also in Fig. 1 is a graph showing the incident flux distribution for various deposition techniques. θ is defined as the angle between the surface normal and the direction of the incidence beam of atoms.

In many applications of thin-films, it is often desired to have atomically flat surfaces. However, in almost all of the deposition techniques mentioned above (except MBE), the surface morphology generates a growth front roughness. The formation of growth front is a complex phenomenon and very often occurs far from equilibrium. When atoms are deposited on a surface, atoms do not arrive at the surface at the same time uniformly across the surface. This random fluctuation, or noise, which is inherent in the process, may create the surface roughness. The noise competes with surface smoothing processes, such as surface diffusion (hopping), to form a rough morphology if the experiment is performed at either a sufficiently low temperature or at a high growth rate. For example, at low surface diffusion rates, random clustering of atoms at initial stages of the growth can lead to a wide range of island sizes followed by side-wall growth of these clusters.[12,14,15] This process results in a rough morphology with fan shaped columnar features observed at the film cross-section, which is depicted as a Zone-1 film in Thornton's well known structure zone model (SZM, which qualitatively describes microstructure of sputter deposited thin-films as a function of temperature and working gas pressure).[12,16–18]

A conventional statistical mechanics treatment cannot be used to describe the complex phenomenon of surface morphology formation in thin-film growth. In 1985, Family and Vicsek introduced a dynamic scaling approach[19,20] to describe the morphological evolution of a growth front. Dynamic scaling theory treats the growing surface having a fractal morphology, which

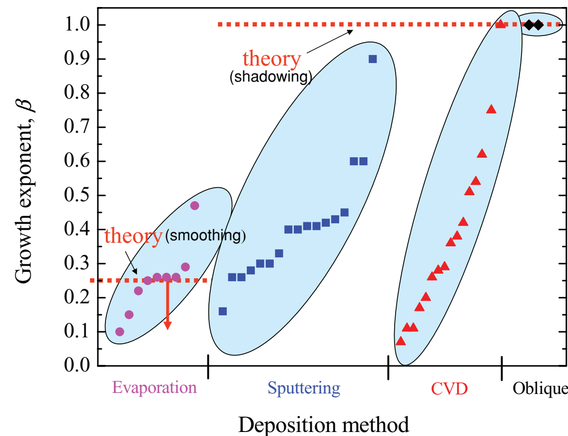

Fig. 2 A survey of experimentally obtained values of growth exponent β reported in the literature for different deposition techniques is compared to the predictions of common thin-film growth models in dynamic scaling theory. rms roughness grows as a function of time in a power law form, $\omega \sim t^{\beta}$, where β is the "growth exponent" ranging between 0 and 1. $\beta = 0$ for a smooth growth front and $\beta = 1$ for a very rough growth front. Reprinted with permission from Ref. 26. Copyright 2009, American Physical Society.

can occur as a result of competition between local smoothening effects (e.g., surface diffusion) and random fluctuations during growth. Because of the fractal property, it is expected that morphology of the thin-film should incorporate similar surface features when investigated at different length scales. In addition, dynamic scaling theory predicts that surface roughness can be scaled with time, which implies the dynamic invariance of surface features. Depending on the type of surface smoothening mechanism, scaling of surface morphology through space and time can be defined by a unique set of "scaling exponents." Since 1985, numerous modeling and experimental works have been reported based on the dynamic scaling analysis.[2,3] One common aim of these models was to predict scaling exponents, which would not depend on the experimental details of the growth process such as type of the material used, temperature, or deposition rate of the incident flux of atoms. By this way, researchers attempted to discover "universal" growth models with a special set of scaling exponents that can define a large variety of experimentally grown thin-film morphologies.

On the other hand, there has been a significant discrepancy among the predictions of these growth models and the experimental results published.[4,21–23] For example, various growth models have predictions on the dynamic evolution of the root-mean-square (rms) roughness,[24] which is defined as $\omega(t) = \sqrt{[h(r,t) - \langle h \rangle]^2}$, where $h(r,t)$ is the height of the surface at a position r and time t, and $\langle h \rangle$ is the average height at the surface. In most of the growth phenomena, the rms grows as a function of time in a power law form,[2,3,25] $\omega \sim t^{\beta}$, where β is the "growth exponent" ranging between 0 and 1. $\beta = 0$ for a smooth growth front and $\beta = 1$ for a very rough growth front.

Figure 2 shows a collection of experimental β values reported in the literature[26] and compares to the predictions of some well known growth models. Briefly, theoretical predictions of growth models in dynamic scaling theory basically fall into two categories. One involves various surface smoothing effects, such as surface diffusion, which lead to $\beta \leq 0.25$[2,3,25] The other category involves the shadowing effect (which originates from the preferential deposition of obliquely incident atoms on higher surface points and always occurs in sputtering and CVD) during growth which would lead to $\beta = 1$.[27] However, it can be clearly seen in Fig. 2 that experimentally reported values of growth exponent β are far from agreement with the predictions of these growth models. Especially, sputtering and CVD techniques are observed to produce morphologies ranging from very small to very large β values indicating a "nonuniversal" behavior.

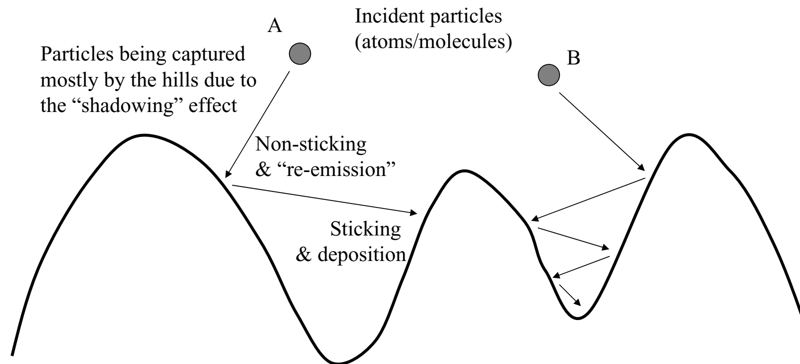

Fig. 3 Surface of a growing thin-film under shadowing and re-emission effects is illustrated. Reprinted with permission from Ref. 26. Copyright 2009, American Physical Society.

2 Shadowing and Re-Emission Effects

Only recently, it has been recognized that in order to better explain the dynamics of surface growth during important deposition methods such as sputtering and CVD, one should take into account the effects of both "shadowing" and "re-emission" processes. [21,23, 28–32] As illustrated in Fig. 3, during growth, particles can approach the surface at oblique angles and be captured by higher surface points (hills) due to the shadowing effect. This leads to the formation of rougher surfaces with columnar structures that can also be engineered to form "nanostructures" under extreme shadowing conditions, as in the case of oblique angle deposition that can produce arrays of nanorods and nanosprings.[7–12] Shadowing can also occur even at atomic scales (so-called "atomic shadowing effect") and can cause side-wall growth of surface features during ballistic deposition of normal angle growth.[3]

In addition, depending on the detailed deposition process, particles can either stick to or be "re-emitted" (bounced off) from their impact points, which is determined by a sticking probability, also named "sticking coefficient" (s). Sticking coefficient is the overall likelihood of an atom/molecule sticking to the surface after complicated physical and chemical processes (e.g., physical reflection, physisorption, chemisorption, and desorption), and therefore represents a statistical average property of the incident flux interaction with the growing surface. The value of sticking coefficient and detailed energy and flux distribution of re-emitted particles can strongly depend on the experimental growth parameters used (e.g., growth temperature, energy of the incident particle, and angle of the incident flux) as well as to local surface morphology. In the case of a relatively high energy incident flux (e.g., > 50 eV for copper), re-emission can also originate indirectly from a resputtering process.[12,30–32] Resputtering includes a surface atom being knocked off by an energetic ion/atom followed by redeposition on a valley of the surface.

Nonsticking particles are re-emitted and can arrive at other surface points including shadowed valleys as illustrated in Fig. 3. In other words, re-emission has a smoothening effect while shadowing tries to roughen the surface. Both the shadowing and re-emission effects have been proven to be dominant over the surface diffusion and noise, and act as the main drivers of the dynamical surface growth front.[10,11] The prevailing effects of shadowing and re-emission rely on their "nonlocal" character: The growth of a given surface point depends on the heights of near and far-away surface locations due to shadowing and existence of re-emitted particles that can travel over long distances.

Figure 4 summarizes some of the experimentally measured sticking coefficient values reported in the literature during evaporation,[33] sputtering,[34–41] and CVD[42–48] growth of various thin-film materials. Names of incident atoms/molecules on the growing film are also labeled. It can be clearly seen from Fig. 4 that incident particles can have sticking probabilities much less

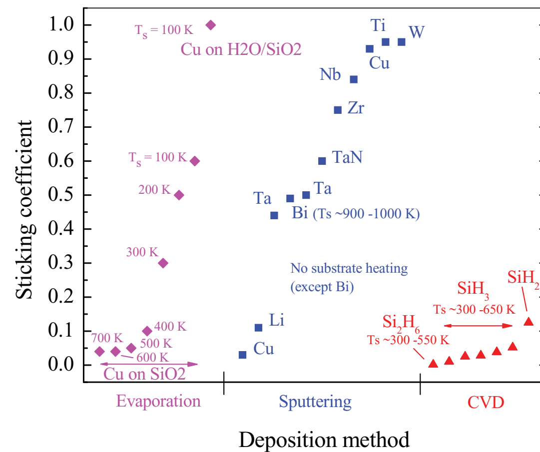

Fig. 4 Some of the experimentally measured sticking coefficient values reported in the literature during evaporation (Ref. 33), sputtering (Refs. 34–41, and CVD (Refs. 42–48) growth are shown. Names of incident atoms/molecules on the growing film are also labeled. In same cases, depositions were done at with substrate heating at temperatures denoted as T_s in the figure. Reprinted with permission from Ref. 26. Copyright 2009, American Physical Society.

than unity in many commonly used deposition systems, which further indicates that re-emission effects should be taken into account in attempts for a realistic thin-film growth modeling.

3 Continuum Models

Due to the complexity of the shadowing and re-emission effects, no growth model has been developed yet within the framework of dynamical scaling theory that takes into account both these effects and still that can be analytically solved to predict the scaling exponents and morphological evolution of thin-film or nanostructure deposition. Hamaguchi and Rossnagel were able to develop a continuum model for the special case of trench-filling during ionized magnetron sputtering, which included the effects of shadowing and re-puttering (i.e., similar to re-emission as explained above).[30–32] However, this model was not used to investigate the evolution of film morphology on planar substrates and no scaling exponents have been analyzed.

While analytically not solvable, Drotar et al. [49,50] proposed a dynamic growth equation for plasma and reactive ion etching processes that take into the re-emission and shadowing effects (where, in etching, surface atoms are removed instead of being incorporated to the surface as in the case of deposition). Drotar's model is based on the idea of flux re-emission which was previously used by Singh et al. in a plasma etching simulation model.[51] Since the pressure in a typical plasma etching system is on the order of 100 mTorr, the Knudsen number (the ratio of the mean free path of any gas particles to the characteristic length of the surface features) is large. Hence, collisions between particles within surface features can be neglected. Therefore, the etching particles can travel in a straight line until hitting the surface at another point. Drotar's model also assumes that the surface evolves slowly compared to the redistribution of flux due to the surface features. In this model, particles are incident on a surface, and a given particle either etches the surface at the point of incidence or is re-emitted in a direction that depends on the re-emission mode. The probability of an incoming particle sticking to the surface is s_0 ($0 \leq s_0 \leq 1$), where s_0 is called the zeroth order sticking coefficient. Incoming particles are called zeroth order particles, while an n'th order particle that has been re-emitted is called an $(n+1)$th order particle. The probability of an n'th order particle sticking is s_n ($0 \leq s_n \leq 1$), and there is a probability of $(1-s_n)$ that this particle will not stick, but will, instead, go somewhere else (in other words, the flux is redistributed).

Drotar's model assumes a two-dimensional surface described by a height function $h(\boldsymbol{r},t)$, where $\boldsymbol{r} = (x,y)$. Overhangs are not allowed in this model. The overall flux of n'th order particles at in-plane position $\boldsymbol{r}$ at time t is denoted by $F_n(\boldsymbol{r},t)$. Finally, the surface evolution in Drotar's re-emission model can be described by the continuum equation

$$\frac{\partial h}{\partial t} = \nu\nabla^2 h - \kappa\nabla^4 h \mp \sqrt{1 + (\nabla h)^2}\,(s_0 F_0(\mathbf{r}, t) + s_1 F_1(\mathbf{r}, t) + \ldots) + \eta, \tag{1}$$

where the condensation/evaporation term $\nu\nabla^2 h$, the surface diffusion term $-\kappa\nabla^4 h$, and the noise term η have been added in. The inherent noise in the etching or growth process satisfies

$$\langle \eta(\mathbf{r}, t)\rangle = 0, \tag{2}$$

and

$$\langle \eta(\boldsymbol{r}, t)\eta(\boldsymbol{r}', t')\rangle = 2D\delta(\boldsymbol{r} - \boldsymbol{r}')\delta(t - t'), \tag{3}$$

where the sign "$\langle . \rangle$" stands for averaging over space and time, and D sets the magnitude of noise. The minus sign in front of the third term in Eq. (1) indicates an etching process and the plus sign indicates deposition. Also, the model takes into account that the growth or etching takes place in the direction normal to the surface by putting a factor of $\sqrt{1 + (\nabla h)^2}$ in front of the flux terms. The main difficulty lies in finding each F_n. The F_n satisfy, for diffuse re-emission,[49]

$$F_{n+1}(\boldsymbol{r}, t) = (1 - s_n)\int Z(\boldsymbol{r}, \boldsymbol{r}', t)F_n(\boldsymbol{r}', t)\frac{(\hat{\boldsymbol{n}}_{\boldsymbol{r}\boldsymbol{r}'}\cdot\hat{\boldsymbol{n}})P(\hat{\boldsymbol{n}}_{\boldsymbol{r}'\boldsymbol{r}}, \hat{\boldsymbol{n}}')}{(\boldsymbol{r} - \boldsymbol{r}')^2 + (h - h')^2}dA', \tag{4}$$

where $\hat{\boldsymbol{n}}$ is the unit normal pointing out of the surface at position $\boldsymbol{r}$, $\hat{\boldsymbol{n}}'$ is the unit normal at position $\boldsymbol{r}'$, $\hat{\boldsymbol{n}}_{\boldsymbol{r}\boldsymbol{r}'}$ is the unit vector pointing from $\boldsymbol{r}$ to $\boldsymbol{r}'$, and $\hat{\boldsymbol{n}}_{\boldsymbol{r}'\boldsymbol{r}}$ is the unit vector pointing from $\boldsymbol{r}'$ to $\boldsymbol{r}$. $P(\hat{\boldsymbol{n}}_{\boldsymbol{r}'\boldsymbol{r}}, \hat{\boldsymbol{n}}')$ is the probability distribution of the re-emitted flux (the probability per solid angle that the particle will be re-emitted in the given direction) and, for thermal re-emission, is equal to $(\hat{\boldsymbol{n}}_{\boldsymbol{r}'\boldsymbol{r}}\cdot\boldsymbol{n}')/\pi$. $Z(\boldsymbol{r},\boldsymbol{r}',t)$ is equal to one except when there is no line of sight between the surface elements at $\boldsymbol{r}$ and $\boldsymbol{r}'$ or $(\hat{\boldsymbol{n}}_{\boldsymbol{r}\boldsymbol{r}'}\cdot n)$ is negative, in which case Z is zero.

Drotar's model still requires some assumptions for various important unknowns.[49] The first one is the characteristics of F_0. For example, in plasma etching, both chemical etching by radicals and physical bombardment by ions can occur. For chemical etching, radicals can come from all directions (no directionality), i.e., the incoming radicals have a broad angular distribution. However, for ion assisted etching, the ions are directed more perpendicularly to the sample surface. A second important factor in the model is the mode of re-emission.[49] It is necessary to specify the flux distribution profile of re-emitted particles. And another assumption is required for the value of the n'th order sticking coefficient s_n for each n. Because of its complexity, this equation could only be solved numerically for a limited case of re-emission and shadowing scenarios after various simplifications.[49,50] Drotar used this model for plasma etched surfaces assuming $\nu = 0$, $\kappa = 0$, $s_0 = 0.05$, and $s_1 = 1$ for a small lattice size of 128×128.[41] After these simplifications, plasma etching continuum model predicted $\beta = 1$, which agreed well with the results of previous experimental results.[41] However, due to the need for high computational power, this continuum model could not be utilized for modeling thin-film deposition systems, which can require large lattice sizes, a high order re-emission process, and also effects of surface diffusion.[42]

4 Monte Carlo Simulation Methods

In recent years, as an alternative approach to continuum models, shadowing and re-emission effects could be fully incorporated into the Monte Carlo lattice simulation approaches.[4,11,21–23,26,28,29,49,50,52–54] In these simulations, each incident particle (atom,

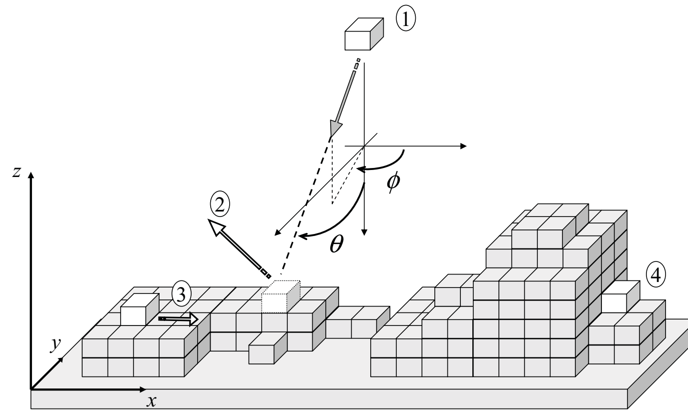

Fig. 5 Some basic processes in the Monte Carlo simulation: (1) A particle is sent toward surface with angles θ *and* ϕ. This particle sticks to the surface with probability s_0. (2) If the particle does not stick, then it is re-emitted. If it finds another surface feature on its way it may stick there with probability s_1. The re-emission process goes on like this for higher-order particles, too. (3) An adatom can diffuse on the surface. (4) Some surface points are shadowed from the incident and re-emission fluxes of particles due to the nearby higher surface features. Reprinted with permission from Ref. 28. Copyright 2001, American Physical Society.

molecule, or a group of atoms) is represented with the dimension of one lattice point (Fig. 5). As substrate, an $N \times N$ size lattice with continuous boundary conditions can be used. A specific angular distribution for the incident flux of particles is chosen depending on the deposition technique being simulated. During normal angle deposition, all the particles are sent from the top along the substrate normal (polar angle $\theta = 0°$), while oblique angle deposition simulations uses a grazing incidence flux where all particles are emitted at an angle θ (e.g., $\sim 85°$), which is measured from the substrate normal.[11,52,53] For CVD and plasma etching, the incident flux can be set to have an angular spread according to the distribution function $dP(\theta,\phi)/d\Omega = \cos\theta/\pi$, where ϕ is the azimuthal angle.[29,49,50] And for sputter deposition simulations, a relatively narrower angular flux distribution with $dP(\theta,\phi)/d\Omega = (2\cos\theta)/(\pi \sin\theta)$ is more appropriate.[28]

As illustrated in Fig. 5, at each simulation step, a particle is sent toward a randomly chosen lattice point on the substrate surface. Depending on the value of sticking coefficient (s), the particle can bounce off and re-emit to other surface points. Re-emission direction can be chosen according to a cosine distribution centered around the local surface normal (Note that depending on the detailed deposition process other types of re-emission modes are also possible such as uniform distribution around the surface normal, specular reflection, or in the case of resputtering it can be according to a cosine distribution centered around the specular direction.).[49] At each impact, sticking coefficient can have different values represented as s_n, where n is the order of re-emission ($n = 0$ being for the first impact). If a constant sticking coefficient value is used for all impacts (i.e., $s_n = s$ for all n), the process is called "all-order re-emission".[49] In all the emission and re-emission processes, shadowing effect is included, where the particle's trajectory can be cut-off by long surface features on its way to other surface points.

After the incident particle is deposited onto the surface, it becomes a so-called "adatom." Adatoms can hop on the surface according to some rules of energy, which is a process mimicking the surface diffusion. One way of introducing surface diffusion is through making D/F number of prescribed surface atoms to "attempt" for hopping when a particle is deposited.[28] D denotes the number of surface atoms ready to diffuse in a given time interval. The time interval is described as the F number atoms deposited on the surface. In a time interval of one deposited atom ($F = 1$) the surface has D number of atoms, which can diffuse. Therefore, at a time step of a deposited single particle, the surface can, at most, have D/F diffusing atoms. In this way,

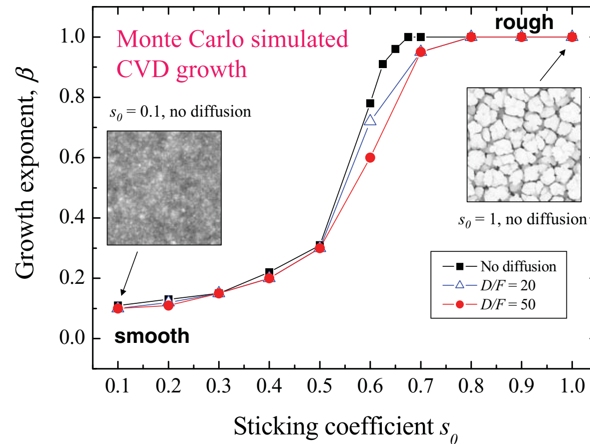

Fig. 6 Growth exponent β values for a Monte Carlo simulated CVD growth obtained for various first-impact sticking coefficient (s_0) and surface diffusion (D/F) values. The sticking coefficient at the second impact after re-emission was set to 1. Two sample surface morphologies having 512×512 lattice size are also included for a small $s_0 = 0.1$ (left) and high $s_0 = 1$ (right) sticking coefficient value, which leads to a smooth and rough surface topography, respectively. Reprinted with permission from Ref. 26. Copyright 2009, American Physical Society.

the ratio of diffusion to deposition strength is adjusted (see the discussion given on p. 176 of Ref. 3). The diffusing surface atom can jump to a nearby site with a probability proportional to $\exp[-(E_0+nnE_N)/k_BT]$. Here E_0 is the activation energy for diffusion, E_N is the bonding energy with a nearest neighbor, and nn is the number of nearest neighbors. k_B and T are the Boltzmann constant and surface temperature, respectively. The particle goes on jumping until it finds an island of atoms, a kink site, a valley or any lattice point, where (E_0+nnE_N) becomes large and the diffusion probability becomes small. The diffusing particle is prohibited from making a single jump up to a site where the height change is more than one lattice atom. But it can diffuse all the way down to surface valleys at any time (i.e., $\Delta h \leq 1$) (Note: The assumption of a particle diffusing along a steep side wall is generally valid for Monte Carlo simulated films due to the coarse-grained property of the simulation technique and is still effective in predicting the top surface morphology of relatively dense films. However, this assumption can fail when "overhangs" become important such as in the case of oblique angle deposition of 3D nanostructures or columnar films produced by sputter deposition at high pressures.).[3] After the deposition step in simulation, another particle is sent, and the re-emission and deposition are repeated in a similar way. In Monte Carlo simulations, deposition time t can be represented by the number of particles sent to the surface. Because of re-emission, deposition rate and therefore average film thickness (d) depends on the sticking coefficient s used, and changes with simulation time t approximately according to $d \approx t \times s/(N \times N)$.[26]

Recent Monte Carlo simulation studies[4,11,21–23,26,28,29,49,50,52–54] performed for CVD, plasma etching, sputter growth, and oblique angle deposition processes successfully predicted the experimental results on surface morphology including the β values shown in Fig. 2. Like in experiments, β values from CVD and sputter deposition simulations ranged all the way from 0 to 1 depending on the sticking coefficients used.[26,28,29] For example, Fig. 6 shows β values for a Monte Carlo simulated CVD growth obtained for various sticking coefficient and surface diffusion values.[26] Surface diffusion parameters were set to $E_0 = 0.1$ eV, $E_N = 0.1$ eV, and $T = 350$ K with D/F values varying from 0 to 50. It has been observed that re-emission and shadowing effects dominated over the surface diffusion processes due to their long-range non-local character. At small sticking coefficients (e.g., $s_0 < 0.5$) re-emission was stronger than the roughening effects of shadowing and Monte Carlo simulations produced smooth surfaces with small β values. At higher sticking coefficient values, the shadowing effect becomes the dominant

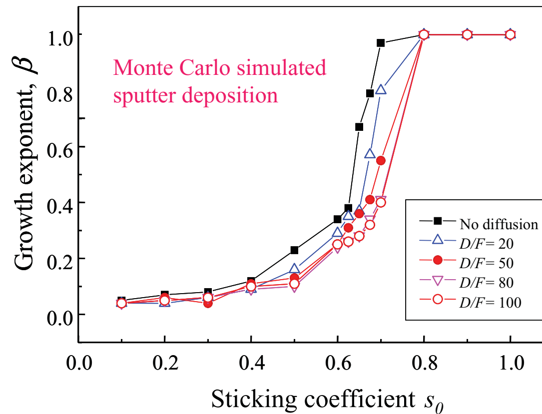

Fig. 7 Growth exponent β values for a Monte Carlo simulated sputter deposition growth obtained for various first-impact sticking coefficient (s_0) and surface diffusion (*D/F*) values. The sticking coefficient at the second impact after re-emission was set to 1. Reproduced with permission from Ref. 4. Copyright 2003, Materials Research Society.

process and columnar rough morphologies start to the form. These Monte Carlo simulations also successively reproduced the morphologies and exponents predicted by the well-known Kardar-Parisi-Zhang (KPZ)[3] model in dynamic scaling theory, for the case where small sticking coefficient particles were re-emitted multiple times and resulted in a conformal growth.[55]

In addition, Fig. 7 shows β values for a Monte Carlo simulated sputter deposition growth obtained for various sticking coefficient and surface diffusion values[4,28] using the similar simulation parameters as described above. However, in sputter deposition a narrower angular flux distribution has been used [i.e., $dP(\theta,\phi)/d\Omega = (2\cos\theta)/(\pi\sin\theta)$].[28] It can be seen from the comparison of Figs. 6 and 7 that for a given sticking coefficient, sputtered films result in slightly smoother surfaces (i.e., smaller β values) compared to CVD. This is due to the relatively narrower angular distribution (i.e., less number of obliquely incident atoms) and therefore reduced shadowing effect in sputtering compared to the CVD. In addition, energetic bombardment of the film surface during sputter deposition can lead to enhanced surface diffusion rates, which can further decrease β values for a given sticking coefficient. More importantly, similar to the CVD growth, the strong dependence of growth exponent β to the sticking coefficient still exists, which can explain diverse β values reported for sputter deposited thin-films in the literature (Fig. 2).

Monte Carlo simulation methods have also been shown to be quite useful in explaining the growth of nanostructured thin-films with unusual crystal orientation/structure under the conditions where shadowing effect is enhanced as in the case of oblique angle deposition.[56–59] Obliquely deposited nanorods have been shown to incorporate non-preferential crystal orientations[57,58] or metastable crystal phases[56,59] at deposition conditions otherwise similar to that of normal incidence grown conventional thin-films with energetically favorable preferential crystal orientations/structures. Briefly, for a Monte Carlo simulation study to investigate this unusual growth behavior, three-dimensional lattice is formed by cubic lattice points and each incident atom had the dimension of one lattice point.[58,59] The simulations include an obliquely incident flux at angle θ, substrate rotation, and surface diffusion. At each simulation step an atom is sent toward a randomly chosen lattice point on the surface of size $N \times N$. To take into account the substrate rotation, each atom is sent with a change in the azimuthal angle of $\Delta\phi$ degrees from the previous one. After the incident atom is deposited onto the surface, an atom that is chosen randomly on the surface is set to diffuse to another nearest neighbor random location according to the diffusion mechanism explained above. To study the crystal orientation/structure evolution, incident atoms are randomly labeled as being either A or B. Therefore, if the particle is deposited on the substrate it forms a nucleation site for A- or B-type crystal

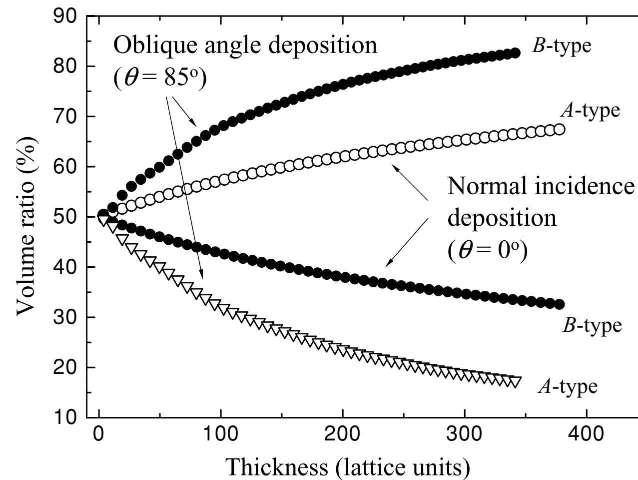

Fig. 8 Evolution of simulated volume ratios of *A*- and *B*-type film sites of different crystal orientation/structure during the oblique angle and normal incidence depositions are shown. The simulation parameters are the same for both the normal incidence and oblique angle deposition except the deposition angle, where $\theta = 0$ deg for the normal incidence and $\theta = 85$ deg for the oblique angle growth. Adatom mobilities are set to be higher on *A*-type islands compared to *B* islands. Common simulation parameters are $N \times N = 512 \times 512$, $\Delta\phi = 0.036$ deg, $T = 358$ K, and $E_D = E_n = 0.05$ eV, $= 0.1$ eV, and $= 0.5$ eV on *A*-type, *B*-type, and substrate surface sites, respectively. Reproduced with permission from Ref. 59. Copyright 2004, Materials Research Society.

orientation/structure with equal probability. However, if it is deposited on an existing island with a specific type of *A* or *B*, then its type is set to this island's type. For the diffusion process, different activation and bond energies for *A*, *B*, and substrate sites are assigned. This mimics the effect of different adatom mobilities that depend on the type of the crystal orientation/structure. In cases where a diffusing adatom moves on top of an island of a different type, the type of the adatom is changed only if the *nn* (number of nearest neighbors) of the other phase outnumbers the *nn* having the same type with the adatom.

Figure 8 shows an example profile for the simulated volume ratios of *A* and *B* sites after high adatom mobilities (i.e., low E_D and E_n) and low adatom mobilities have been assigned to *A*- and *B*-type surface sites, respectively. It is realized that during conventional normal incidence deposition the film structure becomes dominated by the *A*-type as the thickness increases. On the other hand, during the oblique angle growth, the *B*-type islands of low adatom mobility can grow faster in height. Incident particles preferentially deposit on these islands due to the shadowing effect and this leads to the evolution of a dominant *B*-type. These simulation results agree well with the experimental observations.[56–59]

5 Future Directions

As discussed above, Monte Carlo simulation methods that include shadowing and re-emission effects during thin-film growth were quite successful in explaining the diverse experimental results reported in the literature. On the other hand, like in experiments, it was not possible to capture a "universal" growth behavior using Monte Carlo simulation approaches, which would lead to dynamically common aspects of various thin-film growth processes. Universality, which states that the values of surface roughness related scaling exponents such growth exponent β should not depend on the details of the experimental system, has long been predicted by continuum growth models within the framework of dynamic scaling theory.[2,3]

Moreover, it has been recently revealed that shadowing effect can lead to the breakdown of dynamical scaling theory due the formation of a mounded surface morphology.[21–23,60] In these studies, using Monte Carlo simulations it has been shown that for common thin-film deposition techniques, such as sputter deposition and CVD, a "mound" structure can be formed with a characteristic length scale that describes the separation of the mounds, or "wavelength" λ. It has been found that the temporal evolution of λ is distinctly different from that of the mound size, or the lateral correlation length, ξ. The formation of the mound structure is due to non-local growth effects, such as shadowing, that lead to the breakdown of the self-affinity[3] of the morphology described by the dynamic scaling theory. The wavelength grows as a function of time in a power law form, $\lambda \sim t^p$, where $p \approx 0.5$ for a wide range of growth conditions (except for the case of energetic ion bombardment during sputter deposition that leads to formation of narrower columnar features with smaller exponents[12]), while the mound size grows as $\xi \sim t^{1/z}$, where $1/z$ depends on the growth conditions.

We have seen that conventional growth models in dynamic scaling theory cannot explain most of the experimental results reported for dynamic thin-film growth; and dynamic scaling theory itself often suffers from a breakdown if shadowing effect is present, which is the case for most of the commonly used deposition techniques. On the other hand, Monte Carlo simulation techniques were not successful in revealing the possible universal behavior in various growth processes. Therefore, there is a need for alternative modeling approaches for the dynamical growth of thin-film surfaces that can lead to universal growth behavior aspects of thin-films.

Very recently, a new network modeling approach has been proposed for various thin-film growth techniques that incorporates re-emitted particles due to the non-unity sticking coefficients.[26] In this model, re-emission of a particle from one surface site to another is defined to create a network link. Monte Carlo simulations were used to grow films and dynamically track the trajectories of re-emitted particles. Simulations have been performed for normal incidence, oblique angle, and CVD techniques. Each deposition method leads to a different dynamic evolution of surface morphology due to different sticking coefficients involved and different strength of shadowing effect originating from the obliquely incident particles. While traditional dynamic scaling analysis on surface morphology cannot point to any universal behavior, on the other hand, a network analysis reveals that there exist universal behaviors in degree distributions, weighted average degree versus degree, and distance distributions independent of the sticking coefficient used and sometimes even independent of the growth technique.[26] Below we present some of the important details and findings of this network model.

The network model[26] is based on a 3D Monte Carlo simulation method that considers shadowing, re-emission, surface diffusion, and noise effects. These effects simulate the evolution of surface topography and also the simulation environment allows recording trajectories of re-emitted atoms. As an example, Fig. 9 shows the snapshot top view images of two surfaces simulated for a CVD type of deposition at two different sticking coefficients. Figure 9 also displays their corresponding particle trajectories projected on the lateral plane. Qualitative network behavior can easily be realized in these simulated morphologies as the trajectories of re-emitted atoms "link" various surface points. It can also be seen that larger sticking coefficients [Figs. 9(a) and 9(c)] leads to fewer but longer range re-emissions, which are mainly among the peaks of columnar structures. Therefore, these higher surface points act as the "nodes" of the system. This is due to the shadowing effect where initial particles preferentially head on hills. They also have less chance to arrive down to valleys because of the high sticking probabilities. On the other hand, at lower sticking coefficients [Figs. 9(b) and 9(d)], particles now go through multiple re-emissions and can link many more surface points including the valleys that are normally shadowed by higher surface points.

This behavior is better realized in "surface-degree" and their corresponding height matrix plots of Fig. 10 measured for CVD grown films at two different sticking coefficients $s_0 = 0.1$ and $s_0 = 0.9$. The high values (darker colors) in surface-degree plots correspond to the highly connected surface sites where these sites get or redistribute most of the re-emitted particles. At smaller sticking coefficients [Fig. 10(a)], which leads to a smoother morphology,

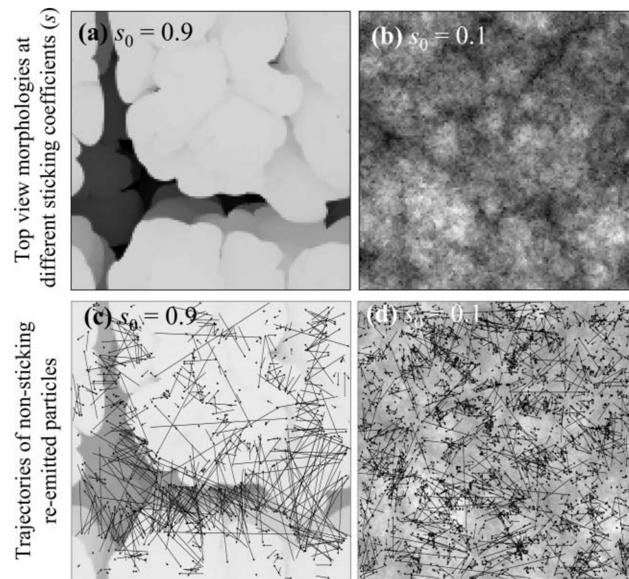

Fig. 9 Top view images from Monte Carlo simulated thin-film surfaces grown under shadowing, re-emission, and noise effects (no surface diffusion is included in these simulations) for sticking coefficients (a) $s_0 = 0.9$ and (b) $s_0 = 0.1$ and with unity sticking coefficient at the second impacts ($s_1 = 1$). The incident flux of particles has an angular distribution designed for CVD. Corresponding projected trajectories of the re-emitted particles are also mapped on the top view morphologies for (c) $s_0 = 0.9$ and (d) $s_0 = 0.1$. Qualitative network behavior can be seen among surface points linked by the re-emission trajectories. Reprinted with permission from Ref. 26. Copyright 2009, American Physical Society.

surface-degree values are quite uniform indicating a uniform re-emission process among hill-to-hills and hill-to-valleys. On the other hand, at high sticking coefficients [Fig. 10(b)], the high degree nodes are mainly located around the column borders suggesting a dominant column-to-column re-emission. This is consistent with the shadowing effect where columns capture most of the incident particles because of their larger heights, and also their borders are more likely to re-distribute the particles toward the neighboring column sides because of the re-emission process used (i.e., cosine distribution centered along the local surface normal).

A more quantitative analysis on the network characteristics of thin-film growth dynamics can be seen in the plots of degree distributions $P(k)$ [i.e., proportional to the percentage of surface points having "degree (k)" number of links through incoming or outgoing re-emitted particles] versus degree k (i.e., the average "lateral" distance particles travel that are re-emitted from/to surface cites having k number of links). Figure 11 plots degree distribution profiles for Monte Carlo simulated films of normal incidence evaporation, oblique angle deposition, and CVD for various sticking coefficients. Figures 11(a) and 11(b) correspond to the initial (thinner films) and later (thick films) stages of the growth times, respectively. First, the comparison of degree distributions [Figs. 11(a) and 11(b)] of normal incidence and oblique angle growth reveals that independent of the most sticking coefficients used and also their growth time, universal behavior exists for both deposition techniques: There is an exponential degree distribution for normal angle evaporation (confirmed in the semi-log plots, not shown here), while this behavior is mainly power-law for oblique angle deposition with an exponential tail. Interestingly, quantitative values of degree distributions for both normal and oblique angle depositions also seem to be independent of the sticking coefficient used, which becomes clearer at later stages of the growth [Fig. 11(b)], leading to two distinct distributions for each deposition. The power-law observed in degree distribution of oblique angle deposition has a $P(k) \sim k^{-2}$ behavior apparent at later stages. All these suggest the possibility of a universal behavior in normal and oblique

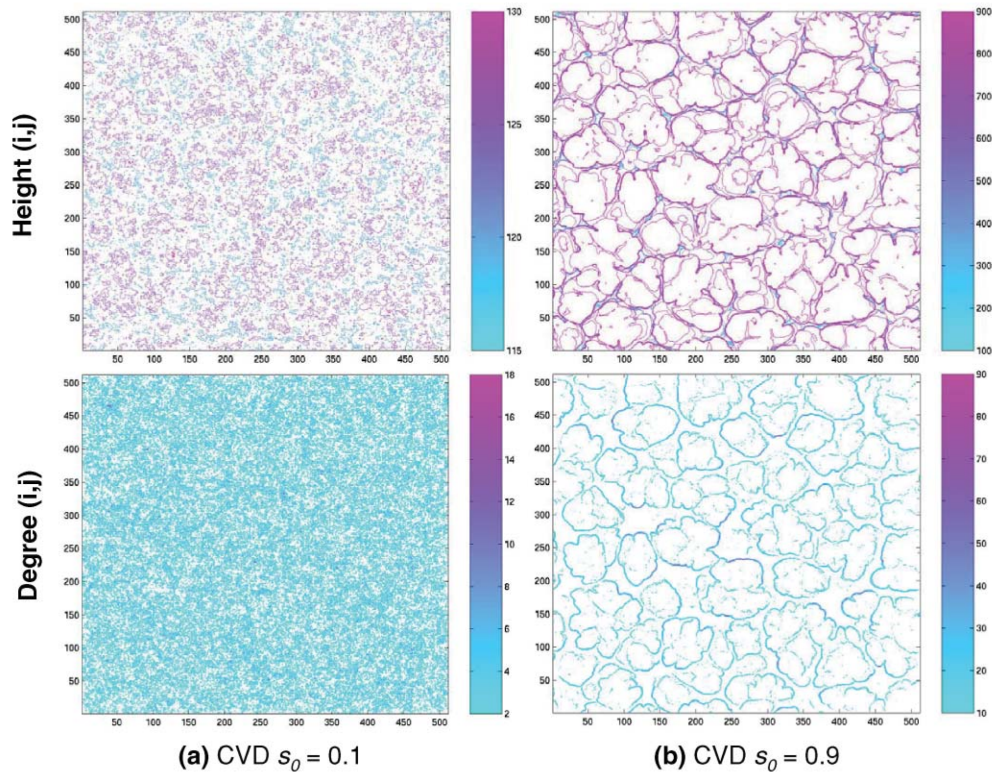

Fig. 10 Height matrix and corresponding surface-degree values are plotted for CVD grown films with sticking coefficients (a) $s_0 = 0.1$ and (b) $s_0 = 0.9$. Simulation time for these snapshot states was $t = 23.75 \times 10^7$ particles. Reprinted with permission from Ref. 26. Copyright 2009, American Physical Society.

angle growth independent of the sticking coefficient. This is quite striking since each different sticking coefficient corresponds to a different type of morphological growth (i.e., smoother surfaces for smaller sticking coefficients and rougher surfaces for higher sticking coefficients), yet the degree distribution in network traffic of re-emitted particles seems to reach a unique universal state.

As can be seen in Figs. 11(a) and 11(b), the re-emission process which is the dominant process in normal angle growth promotes an exponential degree distribution; while shadowing which is the governing effect during oblique angle deposition leads to a power-law distribution. On the other hand, CVD shows an exponential degree distribution at initial times of the growth, while it becomes closer to power-law type for higher sticking coefficients $s > 0.5$. This is believed to be competing forces of re-emission and shadowing effects, where the re-emission is more dominant for smaller sticking coefficients and at initial times of the growth when the film is smoother, leading to an exponential degree distribution. However, shadowing effect originating from the obliquely incident particles within the angular distribution of CVD flux can lead to a power-law behavior at higher sticking coefficients especially when the film gets rougher at later stages of the growth. A power-law degree distribution corresponds to a more correlated network that is consistent with the long-range, column-to-column traffic observed in surface-degree plots of high sticking coefficient CVD above [Fig. 10(b)]. It is also realized that especially for high sticking coefficients, there exist high degree nodes represented with data points at the tails of the degree distributions. These relatively small percentage but highly connected nodes are mainly located at the column edges as seen in surface degree plot of Fig. 10(b) and are likely to be the "hubs" of the network. Therefore, briefly, degree distribution during CVD growth can be similar to the universal line of normal incidence growth for smaller sticking coefficients

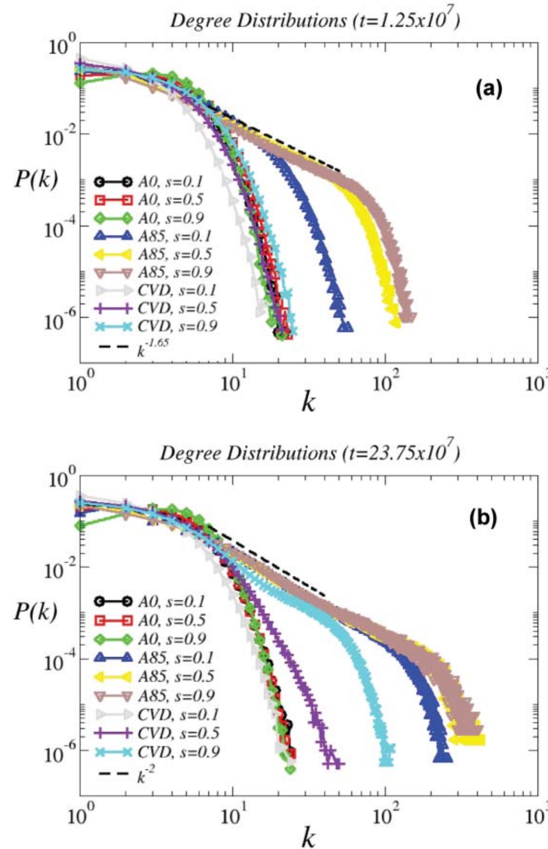

Fig. 11 Behavior of degree distributions $P(k)$ versus degree k for network models of a Monte Carlo simulated normal incidence evaporation (A0), oblique angle deposition (A85), and CVD thin-film growth for various sticking coefficients s and for two different deposition times t (left: $t = 1.25\times10^7$ particles, and right: $t = 23.75\times10^7$ particles) are shown. Reproduced with permission from Ref. 26. Copyright 2009, American Physical Society.

($s < 0.5$) showing an exponential behavior with a short range network traffic; or it can converge to the universal power-law degree distribution of oblique angle deposition for higher sticking coefficients ($s > 0.5$) leading to a highly correlated network driven mostly at column edges.

In addition to the need for new universal growth models, advanced thin-film simulation approaches including detailed atomistic processes would be extremely valuable. One possible method is using molecular dynamics (MD) methods which can incorporate detailed atomistic potentials along with real space dimensions and time. However, MD simulations have not been fully utilized in thin-film growth modeling due to the limited number of atoms involved in the simulations, which cannot typically exceed a few tens of nanometers in scale. In addition, time scales of simulations are also very limited. Advanced computational methods can allow MD simulations of large number of atoms for long time scales that in turn can lead to the modeling of experimentally relevant thin-film sizes and deposition times. If successful, these advanced methods will no longer require the user input parameters such as sticking coefficient values or surface diffusion rates, and instead naturally incorporate these processes during the detailed inter-atomic reactions.

Hybrid modeling approaches such as the ones that incorporates MD simulations into Monte Carlo methods can also provide more near term solutions to some of the limitations of conventional Monte Carlo approaches. For example, Shim et al. recently incorporated MD simulation steps in their Monte Carlo simulations of oblique angle deposition.[61] In order to incorporate

the effect of attraction forces between the substrate atoms and the obliquely incident atom and therefore possible change in the trajectory of the incident atom, they introduced a one-atom MD simulation of the trajectory of the depositing atom (with the substrate atoms all held fixed at their lattice positions) until the distance of the depositing atom to the closest substrate atom was equal to the nearest-neighbor distance $a_1 = a/\sqrt{2}$ (where a is the crystal lattice constant). Similar approaches can also be developed for the re-emission process, where the decision on sticking or nonsticking can be decided based on the MD simulation processes incorporated in the Monte Carlo simulation codes.

6 Conclusions

In conclusion, an overview of thin-film growth dynamics with shadowing and re-emission effects has been presented. It has been discussed that many experimentally reported surface roughness results do not agree with the predictions of conventional growth models such as the one from surface diffusion model. On the other hand, different than the assumptions of conventional growth models, it has been shown that shadowing and re-emission effects can co-exist in a typical thin-film growth system along with other effects. Shadowing can originate either from obliquely incident atoms or from an atomic shadowing effect that can occur even during normal angle growth. In both cases, shadowing has a roughening effect due to preferential deposition of incident atoms on higher surface points. Re-emission effect is a result of nonsticking atoms (or resputtered atoms in the case of energetic bombardment of film surface) and has a smoothening effect due to the redistribution of incident flux of atoms toward valleys of the surface. Both of these effects are nonlocal, long-range, and have been shown to be more dominant over local effects such as surface diffusion. Therefore, one needs to involve both shadowing and re-emission effects in order to establish a realistic thin-film growth model. However, due to the complex nature of shadowing and re-emission effects, a continuum model which is fully solvable either by analytical or numerical methods could not be developed up to this date. On the other hand, recent Monte Carlo simulation methods that involve shadowing, re-emission, surface diffusion, and noise effects successfully predicted many experimentally relevant surface roughness evolution results reported in the literature. For example, similar to experimentally grown thin-films by sputter deposition or chemical vapor deposition techniques, rms surface roughness (ω) of Monte Carlo simulated thin-films have evolved with time t according to a power law behavior $\omega \sim t^{\beta}$, with β values ranging from about 0 to 1 for a growth with strong re-emission effects (i.e., low sticking coefficients or in other words higher probability of non-sticking and being re-emitted to another surface point) and a growth with dominant shadowing effects (i.e., with high sticking coefficients), respectively.

However, Monte Carlo simulation methods still require many important processing parameters such as sticking coefficients or surface diffusion rates as external inputs from the user, which are not always available in the literature. In order to avoid these limitations, there is need for more advanced growth models that can include atomistic details of the physical and chemical process. As one of the possible approaches, molecular dynamics simulation methods can provide the capability of modeling a thin-film growth process based on fundamental laws of physical. Molecular dynamics simulations can also be integrated into Monte Carlo methods for computationally fast and practical hybrid simulation codes.

Conventional continuum thin-film growth models have predicted universal single-valued exponents (such as growth exponent $\beta = 0.25$ for a surface diffusion based growth process) independent of the details of the deposition technique used. However, as in experiments, Monte Carlo simulation models that take into account shadowing and re-emission effects revealed that values of such exponents are very diverse and can strongly depend on parameters such as sticking coefficient. Therefore, there is a need for alternative growth modeling approaches that can capture the universal aspects of thin-film growth dynamics. A recently developed network growth model has been presented as an example approach that has been shown to capture some unique aspects of thin-film growth dynamics independent of the details of growth process.

References

1. D. L. Smith, *Thin-Film Deposition: Principles and Practice*, McGraw-Hill, New York (1995).
2. P. Meakin, *Fractals, Scaling, and Growth Far from Equilibrium*, Cambridge University Press, Cambridge, England (1998).
3. A.-L. Barabasi and H. E. Stanley, *Fractal Concepts in Surface Growth*, Cambridge University, Cambridge, England (1995).
4. T.-M. Lu, Y.-P. Zhao, J. T. Drotar, T. Karabacak, and G.-C. Wang, "Novel mechanisms of the growth morphology thin-films," *Mat. Res. Soc. Symp. Proc.* **749**, 3–8 (2003).
5. N. O. Young and J. Kowal, "Optically active fluorite films," *Nature (London)* **183**, 104–105 (1959).
6. T. Motohiro and Y. Taga, "Thin-film retardation plate by oblique deposition," *Appl. Opt.* **28**, 2466–2482 (1989).
7. R. M. Azzam, "Chiral thin solid films: Method of deposition and applications," *Appl. Phys. Lett.* **61**, 3118–3120 (1992).
8. K. Robbie, M. J. Brett, and A. Lakhtakia, "Chiral sculptured thin-films," *Nature (London)* **384**, 616–616 (1996).
9. K. Robbie, G. Beydaghyan, T. Brown, C. Dean, J. Adams, and C. Buzea, "Ultrahigh vacuum glancing angle deposition system for thin-films with controlled three-dimensional nanoscale structure," *Rev. Sci. Instrum.* **75**, 1089–1097 (2004).
10. T. Karabacak and T.-M. Lu, "Shadowing growth and physical self-assembly of 3D columnar structures," in *Handbook of Theoretical and Computational Nanotechnology*, M. Rieth and W. Schommers, Eds., chap. 69, p. 729, American Scientific Publishers, Stevenson Ranch, CA (2005).
11. T. Karabacak, G.-C. Wang, and T.-M. Lu, "Physical self-assembly and the nucleation of 3D nanostructures by oblique angle deposition," *J. Vac. Sci. Technol. A* **22**, 1778–1784 (2004).
12. A. Lakhtakia and R. Messier, *Sculptured Thin-Films: Nanoengineered Morphology and Optics*, SPIE Press, Bellingham, WA (2005).
13. See, for example, Ref. 3, page 231.
14. R. A. Roy and R. Messier, "Evolutionary growth development in SiC sputtered films," *Mater. Res. Soc. Proc.* **38**, 363–370 (1985).
15. R. A. Roy and R. Messier, "Quantitative analysis of thin-film morphology evolution," in *High Performance Ceramic Films and Coatings*, P. Vincenzini, Ed., Elsevier, Amsterdam, Netherlands (1991).
16. J. A. Thornton, "Influence of apparatus geometry and deposition conditions on the structure and topography of thick sputtered coatings," *J. Vac. Sci. Tech.* **11**, 666–670 (1974).
17. J. A. Thornton, "High rate thick film growth," *Annu. Rev. Mater. Sci.* **7**, 239–260 (1977).
18. R. Messier, A. P. Giri, and R. A. Roy, "Revised structure zone model for thin-film physical structure," *J. Vac. Sci. Technol. A* **2**, 500–503 (1984).
19. F. Family and T. Vicsek, "Scaling of the active zone in the Eden process on percolation networks and the ballistic deposition model," *J. Phys. A* **18**, L75–81 (1985).
20. F. Family, "Scaling of rough surfaces: effects of surface diffusion," *J. Phys. A* **19**, L441–446 (1986).
21. M. Pelliccione, T. Karabacak, and T.-M. Lu, "Breakdown of dynamic scaling in surface growth under shadowing," *Phys. Rev. Lett.* **96**, 146105 (2006).
22. M. Pelliccione, T. Karabacak, C. Gaire, G.-C. Wang, and T.-M. Lu, "Mound formation in surface growth under shadowing," *Phys. Rev. B* **74**, 125420 (2006).
23. M. Pelliccione and T.-M Lu, *Evolution of Thin-Film Morphology: Modeling and Simulations*, Springer, New York (2007).
24. Y.-P. Zhao, G.-C. Wang, and T.-M. Lu, *Characterization of Amorphous and Crystalline Rough Surfaces: Principles and Applications*, Academic Press, San Diego (2001).
25. F. Family and T. Viscek, *Dynamics of Fractal Surfaces*, World Scientific, Singapore (1991).

26. T. Karabacak, H. Guclu, and M. Yuksel, "Network behavior in thin-film growth dynamics," *Phys. Rev. B* **79**, 195418 (2009).
27. R. P. U. Karunasiri, R. Bruinsma, and J. Rudnick, "Thin-film growth and the shadow instability," *Phys. Rev. Lett.* **62**, 788–791 (1989).
28. T. Karabacak, Y.-P. Zhao, G.-C. Wang, and T.-M. Lu, "Growth front roughening in amorphous silicon films by sputtering," *Phys. Rev. B* **64**, 085323 (2001).
29. T. Karabacak, Y.-P. Zhao, G.-C. Wang, and T.-M. Lu, "Growth front roughening in silicon nitride films by PECVD," *Phys. Rev. B* **66**, 075329 (2002).
30. S. Hamaguchi and S. M. Rossnagel, "Simulations of trench-filling profiles under ionized magnetron sputter metal deposition," *J. Vac. Sci. Technol. B* **13**, 183–191 (1995).
31. S. Hamaguchi and S. M. Rossnagel, "Liner conformality in ionized magnetron sputter metal deposition processes," *J. Vac. Sci. Technol. B* **14**, 2603–2608 (1996).
32. C. A. Nichols, S. Hamaguchi, and S. M. Rossnagel, "Ionized physical vapor deposition of Cu for high aspect ratio damascene trench fill applications," *J. Vac. Sci. Technol. B* **14**, 3270–3275 (1996).
33. X. Xu and D. W. Goodman, "Metal deposition onto oxides: An unusual low initial sticking probability for copper on $Si0_2$," *Appl. Phys. Lett.* **61**, 1799–1801 (1992).
34. E. M. van Veldhuizen and F. J. de Hoog, "Analysis of a Cu-Ne hollow cathode glow discharge at intermediate currents," *J. Phys. D: Appl. Phys.* **17**, 953–968 (1984).
35. A. Bogaerts, J. Naylor, M. Hatcher, W. J. Jones, and R. Mason, "Influence of sticking coefficients on the behavior of sputtered atoms in an argon glow discharge: Modeling and comparison with experiment," *J. Vac. Sci. Technol. A* **16**, 2400–2410 (1998).
36. K. Obara, Z. Fu, M. Arima, T. Yamada, T. Fujikawa, N. Imamura, and N. Terada, "Collision processes between sputtered particles on high speed rotating substrate and atomic mass dependence of sticking coefficient," *J. Crystal Growth* **237–239**, 2041–2045 (2002).
37. S. Migita, K. Sakai, H. Ota, Z. Mori, and R. Aoki, "The influence of Bi-sticking coefficient in the growth of Bi(2212) thin-film by ion beam sputtering," *Thin Solid Films* **281–282**, 510–512 (1996).
38. A. Bogaerts, E. Wagner, B. W. Smith, J. D. Winefordner, D. Pollmann, W. W. Harrison, and R. Gijbels, "Three-dimensional density profiles of sputtered atoms and ions in a direct current glow discharge: experimental study and comparison with calculations," *Spectrochim. Acta Part B* **52**, 205–218 (1997).
39. A. J. Toprac, B. P. Jones, J. Schlueter, and T. S. Cale, "Modeling of collimated titanium nitride physical vapor deposition using a combined specular-diffuse formulation," *Mat. Res. Soc. Symp. Proc.* **355**, 575–580 (1995).
40. O. Yamazaki, K. Iyanagi, S. Takagi, and K. Nanbu, "Modeling of Cu transport in sputtering using a Monte Carlo simulation," *Jpn. J. Appl. Phys.* **41**, 1230–1234 (2002).
41. D. Liu, S. K. Dew, M. J. Brett, T. Smy, and W. Tsai, "Compositional variations in Ti-W films sputtered over topographical features," *J. Appl. Phys.* **75**, 8114–8120 (1994).
42. R. J. Buss, P. Ho, W. G. Breiland, and M. E. Coltrin, "Reactive sticking coefficients of silane on silicon," in *Deposition and Growth: Limits for Microelectronics*, G. W. Rubloff, Ed, AIP Conf. Proc. **167**, 34–42 (1988).
43. R. J. Buss, P. Ho, W. G. Breiland, and M. E. Coltrin, "Reactive sticking coefficients for silane and disilane on polycrystalline silicon," *J. Appl. Phys.* **63**, 2808–2819 (1988).
44. C. C. Tsai, J. G. Shaw, B. Wacker, and J. C. Knights, "Film growth mechanisms of amorphous silicon in diode and triode glow discharge systems," *Mat. Res. Soc. Symp. Proc.* **95**, 219–224 (1987).
45. J. Perrin and T. Broekhuizen, "Modelling of $Hg(^3P_1)$ photosensitization of SiH_4 and surface reactions of the SiH_3 radical," *Mat. Res. Soc. Symp. Proc.* **75**, 201–208 (1987).
46. J. Perrin and T. Broekhuizen, "Surface reaction and recombination of the SiH_3 radical on hydrogenated amorphous silicon," *Appl. Phys. Lett.* **50**, 433–435 (1987).

47. R. Robertson and A. Gallagher, "Mono- and disilicon radicals in silane and silane-argon DC discharges," *J. Appl. Phys.* **59**, 3402–3411 (1986).
48. J. Robertson, "Growth mechanism of hydrogenated amorphous silicon," *J. Non-Cryst. Solids* **266–269**, 79–83 (2000).
49. J. T. Drotar, Y.-P. Zhao, T.-M. Lu, and G.-C. Wang, "Mechanisms for plasma and reactive ion etch-front roughening," *Phys. Rev. B* **61**, 3012–3021 (2000).
50. J. T. Drotar, Y.-P. Zhao, T.-M. Lu, and G.-C. Wang, "Surface roughening in shadowing growth and etching in 2+1 dimensions," *Phys. Rev. B* **62**, 2118–2125 (2000).
51. V. K. Singh, E. S. G. Shaqfeh, and J. P. McVittie, "Simulation of profile evolution in silicon reactive ion etching with re-emission and surface diffusion," *J. Vac. Sci. Technol. B* **10**, 1091–1104 (1992).
52. T. Karabacak, J. P. Singh, Y.-P. Zhao, G.-C. Wang, and T.-M. Lu, "Scaling during shadowing growth of isolated nano-columns," *Phys. Rev. B* **68**, 125408 (2003).
53. T. Karabacak, G.-C. Wang, and T.-M. Lu, "Quasi-periodic nano-structures grown by oblique angle deposition," *J. Appl. Phys.* **94**, 7723–7728 (2003).
54. T. Smy, D. Vick, M. J. Brett, S. K. Dew, A. T. Wu, J. C. Sit, and K. D. Harris, "Three-dimensional simulation of film microstructure produced by glancing angle deposition," *J. Vac. Sci. Technol. A* **18**, 2507–2512 (2005).
55. J. T. Drotar, Y.-P. Zhao, T.-M. Lu, and G.-C. Wang, "Why is KPZ type surface roughening so hard to observe?," *Mat. Res. Soc. Symp. Proc.* **648**, P7.9.1-6 (2001).
56. T. Karabacak, A. Mallikarjunan, J. P. Singh, D.-X. Ye, G.-C. Wang, and T.-M. Lu, "β-phase W nanorod formation by oblique-angle sputter deposition," *Appl. Phys. Lett.* **83**, 3096–3098 (2003).
57. P. Morrow, F. Tang, T. Karabacak, P.-I. Wang, D.-X. Ye, G.-C. Wang, and T.-M. Lu, "Texture of Ru columns grown by oblique angle sputter deposition," *J. Vac. Sci. Technol. A* **24**, 205–215 (2006).
58. D. Deniz, T. Karabacak, and J. M. E. Harper, "Competitive growth mechanisms of aluminum nitride thin-films deposited by off-normal reactive magnetron sputtering," *J. of Appl. Phys.* **103**, 083553 (2008).
59. T. Karabacak, P.-I. Wang, G.-C. Wang, and T.-M. Lu, "Growth of single crystal tungsten nanorods by oblique angle sputter deposition," *Mat. Res. Soc. Symp. Proc.* **788**, 75–80 (2004).
60. J. M. Garcia-Ruiz, A. Lakhtakia, and R. Messier, "Does competition between growth elements eventually eliminate self-affinity?," *Speculations Sci. Technol.* **15**, 60–71 (1991).
61. Y. Shim, M. E. Mills, V. Borovikov, and J. G. Amar, "Effects of substrate rotation in oblique-incidence metal(100) epitaxial growth," *Phys. Rev. E* **79**, 051604 (2009).

Tansel Karabacak is an assistant professor at University of Arkansas at Little Rock. He received his BS degree in physics at Middle East Technical University in Turkey. He conducted his PhD studies at Rensselaer Polytechnic Institute, Department of Applied Physics, in the field of growth dynamics of thin-film coatings and oblique/glancing angle deposited (GLAD) nanostructures. His doctoral research led to various awards including American Vacuum Society Graduate Research Award. After he got his PhD degree in 2003, he worked on various projects on the properties and applications of thin-films and GLAD nanostructures. He is the author and co-author of about 50 journal papers, 20 conference proceedings, 1 book chapter, 1 patent, and several pending patents.